Appl. Phys. B 68, 67–72 (1999)

Applied Physics B
Lasers
and Optics

Excited state absorption and stimulated emission of Nd^{3+} in crystals III: $LaSc_3(BO_3)_4$, $CaWO_4$, and $YLiF_4$

L. Fornasiero, T. Kellner, S. Kück, J.P. Meyn*, P.E.-A. Möbert, G. Huber

Universität Hamburg, Institut für Laser-Physik, Jungiusstraße 9a, D-20355 Hamburg, Germany
(Fax: +49-40/4123-6281, E-mail: fornasiero@physnet.uni-hamburg.de)

Received: 8 May 1998/Revised version: 7 September 1998

Abstract. In this paper excited state absorption (ESA) spectra of Nd^{3+} ions in $CaWO_4$, $LaSc_3(BO_3)_4$, and $YLiF_4$ crystals are presented. The spectra were measured by a continuous-wave pump and probe technique. It is shown that ESA is a negligible loss mechanism in cw lasers emitting at 1.06 μm. In contrast, the effective emission cross sections in Nd:$CaWO_4$ and Nd:$LaSc_3(BO_3)_4$ around 1.35 μm are considerably diminished.

PACS: 42.55.P,R; 42.55.Rz; 42.70.H; 71.55.i; 78.45.+h

Absorption from excited states (ESA) can be a considerable loss mechanism for stimulated emission in solid-state lasers. Although ESA spectra had been published on several rare-earth- or transition-metal-doped optical materials, few quantitative data are known about the strength of ESA in Nd^{3+} doped crystals. The aim of this paper is to compare the ESA of Nd^{3+} in $CaWO_4$ (CWO), $YLiF_4$ (YLF), and $LaSc_3(BO_3)_4$ (LSB) and evaluate its implication on the laser efficiency.

Doped $CaWO_4$ is a well-known gain material for solid-state lasers [1–4]. CWO crystals can be grown in high optical quality. Colour centre formation limits the use of Nd:CWO in flashlamp-pumped systems [5], but nowadays the material gains new interest due to its broad absorption lines, which facilitate diode pumping.

$YLiF_4$ is isomorphic to CWO. Both crystals have the tetragonal scheelite structure with symmetry 4/m (Hermann–Mauguin notation). The similarity of rare-earth ion spectra in YLF and CWO has already been stated in the past and motivates a comparison of the ESA in both materials. However, Nd:YLF shows narrow absorption and emission lines with about 15 cm^{-1} FWHM at 300 K [6]. The use of Nd:YLF in lasers dates back to 1967 [7]. The crystal has a high resistance to solarization under flashlamp pumping [8]. The long lifetime of the Nd^{3+} metastable state $^4F_{3/2}$ of 570 μs [9] permits storage of high energies and makes Nd:YLF an attractive material for Q-switched laser operation. In the Q-switched mode the peak inversion of the gain material exceeds considerably the inversion that is reached in resonators with high Q-factors. Since ESA increases with the population of the metastable states, ESA on the pump wavelength might also become a considerable loss process in the Q-switched mode. Earlier research on this subject is described in [10–13].

Nd:$LaSc_3(BO_3)_4$ competes with Nd:CWO as gain medium for low-cost simple all-solid-state lasers [14–16]. Nd:LSB and Nd:CWO exhibit broad lines. The absorption band around 800 nm can be pumped by diodes without special temperature stabilisation. On the other hand the effective cross sections of the broad emission lines can be reduced by broad ESA bands as it is observed in Nd:glass [17]. Measurements can clarify if ESA reduces the tunability range or the efficiency of Nd:LSB and Nd:CWO lasers.

This publication is the third part of a series of three papers which gives an overview about ESA in the most important neodymium doped laser crystals. In parts I and II we have described the ESA of Nd-doped $Y_3Al_5O_{12}$, $YAlO_3$, and Y_2O_3, and of YVO_4, $GdVO_4$, and $Sr_5(PO_4)_3F$, respectively [18, 19].

1 Spectroscopic methods

The 300 K gain-ESA measurements were performed with a pump and probe technique in a double modulation scheme as described in [20, 21] and in part I and II of this series. The investigated samples were a Nd(2 at. %):CWO, a Nd(1 at. %):YLF, and a Nd(10 at. %):LSB crystal. The CWO and the LSB crystals were pumped near 800 nm with a laser diode (SDL-2362). The diode emission wavelength was temperature-tuned to the maximum absorption of the crystals. The YLF sample was pumped by an argon ion laser at 514 nm. This allowed us to perform measurements on the absorption band around 800 nm where ESA might become important in the Q-switched mode.

The probe radiation was provided by a broad-band tungsten halogen lamp in all measurements. The transmitted intensities were measured with a Si detector (850–1100 nm)

* *Present address*: Universität Kaiserslautern, Erwin-Schrödinger-Str. 46, D-67661 Kaiserslautern, Germany

or a liquid-nitrogen-cooled InSb detector (1000–1500 nm), which were placed behind a 0.5 m monochromator.

The resolutions of the gain-ESA spectra are about 0.8 nm between 850 nm and 1100 nm and about 2 nm between 1100 nm and 1500 nm. The precise values are given in the figure captions. The fluorescence spectra of Nd:LSB and Nd:CWO (taken with a similar pumping source, spectrometer, and detector assembly) have a resolution of about 0.2 nm. Because the linewidth of Nd:YLF is too small to be resolved in the gain-ESA spectrum, the respective emission spectrum is given with the same low resolution (0.8 nm) for better comparison.

The data processing was performed as described in part I and II of this series. We assumed that in the pumped system only the $^4F_{3/2}$ metastable state is populated besides the ground state due to the short lifetimes of the other states. It can be shown that under this assumption the following equation holds [21]:

$$\frac{I_\mathrm{p}(\lambda) - I_\mathrm{u}(\lambda)}{I_\mathrm{p}(\lambda)} = k(\sigma_\mathrm{GSA}(\lambda) + \sigma_\mathrm{SE}(\lambda) - \sigma_\mathrm{ESA}(\lambda)) \; . \qquad (1)$$

I_p is the transmitted light intensity when the sample is pumped and I_u when it is not pumped, σ_GSA, σ_SE, and σ_ESA are the cross sections of the GSA, the stimulated emission, and of the ESA, respectively, k is a factor which is the product of the excited ion density and the sample thickness. The measured values of $(I_\mathrm{p} - I_\mathrm{u})/I_\mathrm{p}$ on the left hand side of (1) were calibrated to the corresponding absorption and emission cross sections on the right-hand side of (1) in spectral regions where no ESA is present, i.e. $\sigma_\mathrm{ESA} = 0$.

Emission cross section spectra in the regions of GSA, i.e. on the transition $^4F_{3/2} \rightarrow {}^4I_{9/2}$, were calculated from ground state absorption cross sections using the reciprocity principle of McCumber [22]. The emission cross sections of transitions from the $^4F_{3/2}$ manifold in lower states were obtained by multiplication of the fluorescence spectra with a factor λ^5 (according to the Füchtbauer and Ladenburg relation) and a subsequent normalisation of the spectra on the $^4F_{3/2} \rightarrow {}^4I_{9/2}$ emission cross sections obtained by the reciprocity method.

2 Results and discussion

2.1 Nd*:CWO*

Nd:CWO shows inhomogeneously broadened lines due to the existence of various Na^+ charge-compensated Nd^{3+} classes on the Ca^{2+} sites [3]. The spectral linewidth (FWHM) is about 60 cm^{-1} at 300 K.

The gain-ESA spectra of Nd:CWO are presented in Fig. 1. Positive cross sections are due to stimulated emission, negative ones result from ESA. The radiative transitions around 900 nm ($^4F_{3/2} \rightarrow {}^4I_{9/2}$), at 1058 nm in π- and 1065 nm in σ-polarization ($^4F_{3/2} \rightarrow {}^4I_{11/2}$), and at 1339 nm ($^4F_{3/2} \rightarrow {}^4I_{13/2}$) are clearly observed. The strength of the emission line at 880 nm in the π-polarized spectrum is incorrect because of a high GSA on this line. In this case the transmitted intensity is nearly zero and the expression $(I_\mathrm{p} - I_\mathrm{u})/I_\mathrm{p}$ in (1) becomes very high with a large error margin.

Since to our knowledge only the Stark level energies below 12 000 cm^{-1} are published in the literature [23], we had to estimate the width of the regions where ESA might occur. This was done by measuring the spectral positions of the ground state absorption bands of the higher states at 300 K. From this data the approximate positions of the respective ESA bands from the $^4F_{3/2}$ multiplet were calculated. The $^4F_{3/2} \rightarrow {}^2D_{3/2} + {}^4G_{9/2} + {}^4G_{11/2} + {}^2K_{15/2}$ ESA transitions are expected between 960 nm and 1110 nm, and the $^4F_{3/2} \rightarrow {}^2G_{9/2} + {}^2K_{13/2} + {}^4G_{7/2}$ transitions between 1170 nm and 1420 nm. These regions are indicated by arrows in Fig. 1.

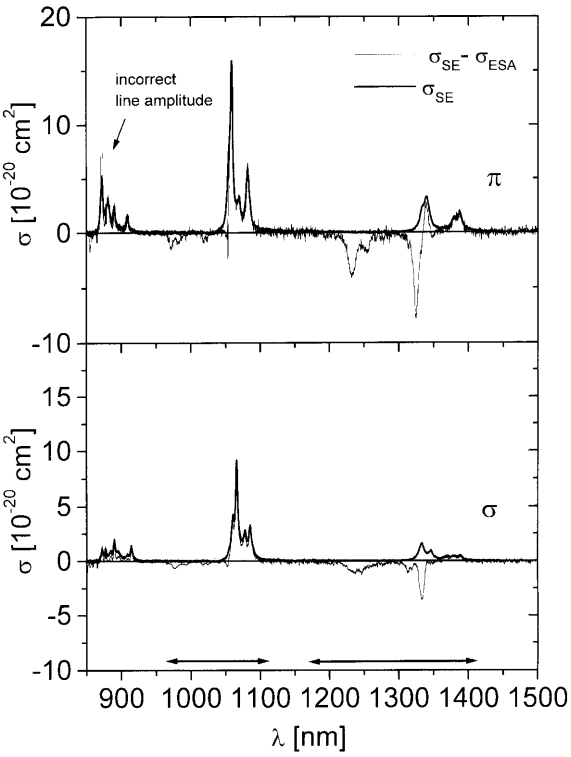

Fig. 1. Polarized gain-ESA spectra $\sigma_\mathrm{SE} - \sigma_\mathrm{ESA}$ (*narrow line*) and emission cross section spectra σ_SE (*bold line*) of Nd:CWO between 850 nm and 1500 nm. Differences between the spectra are due to ESA. The regions of possible ESA transitions starting from the $^4F_{3/2}$ multiplet are indicated by *arrows*. Note that the height of the line at 880 nm in the π-polarized gain-ESA spectrum is not correct (see text)

Looking at the π-polarized spectrum of the $^4F_{3/2} \rightarrow {}^4I_{11/2}$ transition in Fig. 2, an ESA line at 1053 nm is visible in the vicinity of the 1058 nm laser line. For comparison we have added to the spectra the cross sections of stimulated emission determined by the method given in Sect. 1 as a bold line. These emission cross sections agree with the spectra published by Fauré et al. [16]. One can see that a wing of the emission line between 1045 nm and 1055 nm is completely erased. The respective ESA peak cross sections at 1054 nm are about 8×10^{-20} cm^2. However, the laser emission at 1058 nm seems not to be affected.

The most pronounced ESA lines in π-polarization at longer wavelength in Fig. 3 are a double structure with peaks at 1238 nm ($\sigma_\mathrm{ESA} = 4.3 \times 10^{-20}$ cm^2) and 1256 nm ($\sigma_\mathrm{ESA} = 2 \times 10^{-20}$ cm^2) and a very strong line at 1325 nm ($\sigma_\mathrm{ESA} = 8 \times 10^{-20}$ cm^2). ESA lines in σ-polarization are found at 1235 nm, 1245 nm, and 1333 nm. According to the spin selection rule in the Russel–Saunders approximation, i.e. $\Delta S = 0$, these strong lines can be rather attributed to

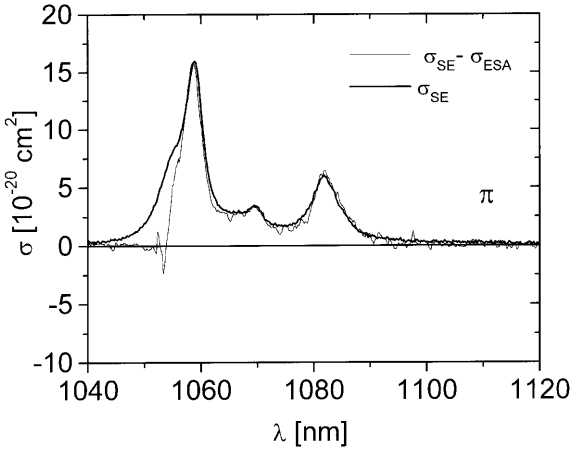

Fig. 2. π-polarized gain-ESA spectrum $\sigma_{SE} - \sigma_{ESA}$ (*narrow line*) and emission cross section spectrum σ_{SE} (*bold line*) of Nd:CWO around 1060 nm. The resolution of the gain-ESA spectrum is 0.9 nm, the resolution of the emission cross section spectrum is 0.2 nm

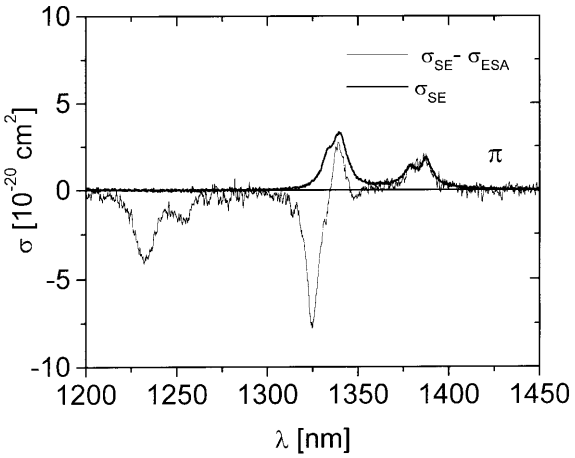

Fig. 3. π-polarized gain-ESA spectrum $\sigma_{SE} - \sigma_{ESA}$ (*narrow line*) and emission cross section spectrum σ_{SE} (*bold line*) of Nd:CWO around 1330 nm. The resolution of the gain-ESA spectrum is 2.2 nm, the resolution of the emission cross section spectrum is 0.2 nm

the ${}^4F_{3/2} \rightarrow {}^4G_{7/2}$ transitions ($S = 4 \rightarrow S = 4$) than to the ${}^4F_{3/2} \rightarrow {}^2G_{9/2} + {}^2K_{13/2}$ transitions ($S = 4 \rightarrow S = 2$). Johnson and Thomas [3] obtained π-polarized laser operation at 1337 nm at 77 K. At room temperature the effective emission peak lies at 1339 nm. This difference could be explained by a broadening of the 1325 nm ESA band that would shift the highest effective cross section to the longer wavelength side when the temperature is increased. However, further temperature-dependent ESA measurements are needed for a proof of this theory.

At its right wing at 1345 nm the stimulated emission band is also erased by ESA with a cross section of about 1×10^{-20} cm^2.

2.2 Nd*:YLF*

Figure 4 shows the gain-ESA spectrum for Nd:YLF between 850 and 1500 nm. Possible ESA transitions starting from the ${}^4F_{3/2}$ manifold are indicated by bars. The corresponding energy values have been taken from da Gama et al. [24]. The

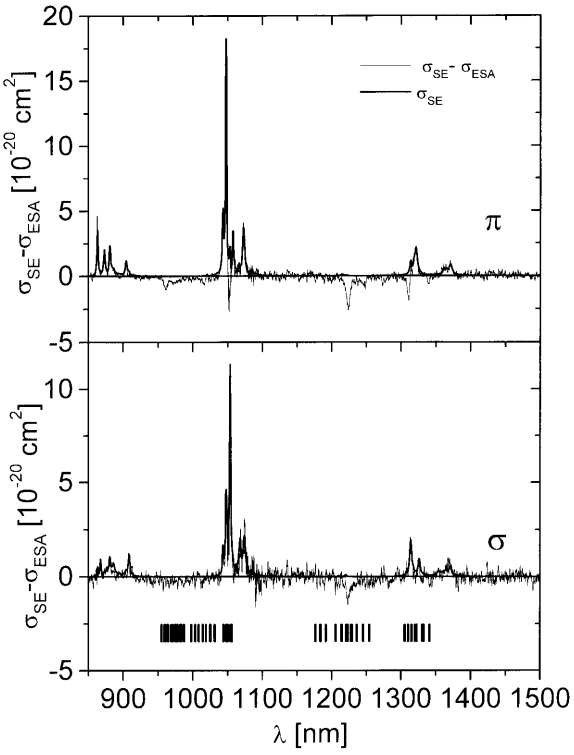

Fig. 4. Polarized gain-ESA spectra $\sigma_{SE} - \sigma_{ESA}$ (*narrow lines*) and emission cross section spectra σ_{SE} (*bold lines*) of Nd:YLF between 850 nm and 1500 nm. The resolution of the gain-ESA spectra is 0.8 nm between 850 nm and 1100 nm and 1.8 nm between 1100 nm and 1500 nm. The resolution of the emission spectra is 0.8 nm. The *bars* indicate the spectral positions of possible ESA transitions starting from the ${}^4F_{3/2}$ multiplet. Note that the peak cross sections appear too small because the narrowest lines are not completely resolved

same crystal structure of YLF and CWO is clearly observed in the similarity of the polarized spectra that has already been stated by Karayanis [25]. The main differences between the gain-ESA spectra of Nd in CWO and YLF are slight variations of the spectral position of the various transitions and the linewidth. Although in highly resolved spectra the strongest emission lines of Nd:YLF near 1.05 μm are higher than the corresponding lines of Nd:CWO, the oscillator strength (which is proportional to the integral of the respective line) is even a little bit smaller. In Fig. 4 the main laser transitions of Nd:YLF are apparent at 1047.1 nm in π- and at 1053 nm in σ-polarization.

The resolution of of the gain-ESA spectra is 0.8 nm under 1100 nm and 2 nm above 1100 nm. The emission spectra have a resolution of about 0.8 nm and are added as bold line graphs in Figs. 4–6. Note, that the narrowest lines could not be fully resolved and that the apparent peak cross sections are too small.

Looking at the 1.06 μm region in Fig. 5 one finds a distinct ESA line in YLF at 1052 nm in π-polarization. Its peak cross section is about 4×10^{-20} cm^2. In σ-polarization ESA seems to exist at 1048 nm on a side line where the difference between the gain-ESA cross section and the emission cross section is estimated to be less than 1×10^{-20} cm^2. The existence of two stronger ESA-lines at 1052 nm in π- and at 1048 nm in σ-polarization is in agreement with the excited state excitation (ESE) spectra measured by Guyot et al. [11]. If we calibrate their better resolved ESE spectra with the

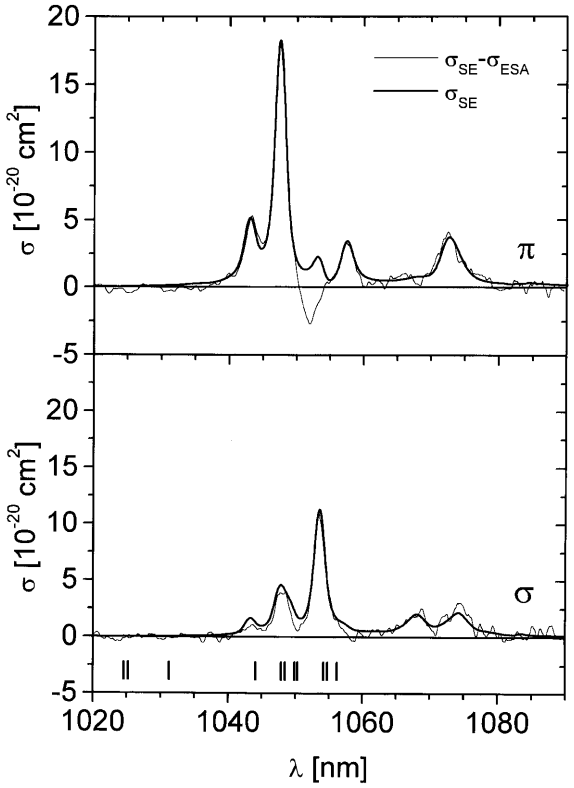

Fig. 5. Polarized gain-ESA spectra $\sigma_{SE} - \sigma_{ESA}$ (*narrow lines*) and emission cross section spectra σ_{SE} (*bold lines*) of Nd:YLF around 1060 nm. The resolution of the spectra is 0.8 nm. The *bars* indicate possible ESA transitions. Note that the peak cross sections appear too small because the corresponding lines are not completely resolved

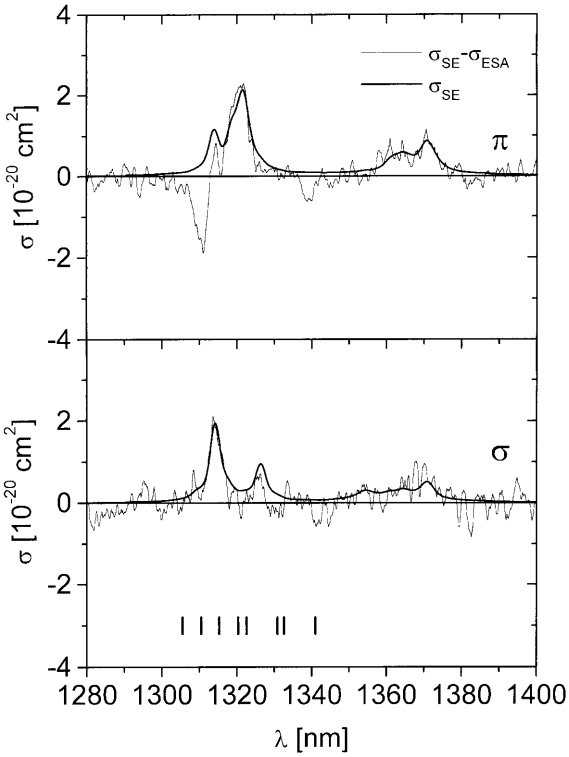

Fig. 6. Polarized gain-ESA spectra $\sigma_{SE} - \sigma_{ESA}$ (*narrow line*) and emission cross section spectra σ_{SE} (*bold line*) of Nd:YLF around 1320 nm. The resolution of the gain-ESA spectrum is 1.8 nm, the resolution of the emission cross section spectrum is 0.8 nm. The *bars* indicate possible ESA transitions

ESA cross sections determined at 1048 nm and 1052 nm, we find an ESA cross section on the laser line in π-polarization at 1047 nm of about 5×10^{-21} cm^2 and on the laser line in σ-polarization at 1053 nm of about 1.5×10^{-21} cm^2. The corresponding ESA lines are not distinctly visible in CWO presumably because of the broader linewidth of Nd^{3+} in this material. ESA is then covered by the much stronger stimulated emission.

ESA lines in Nd:YLF are also found in the 1320 nm region (Fig. 6). They are observed at 1310 nm in π-polarization and at 1340 nm in both polarization directions with cross sections of $\sigma_{ESA} = 2.4 \times 10^{-20}$ cm^2 and $\sigma_{ESA} = 6 \times 10^{-21}$ cm^2, respectively. Calibration of the ESE spectra reported by Guyot et al. [11] with these data yields approximate cross sections of $\sigma_{ESA} = 1 \times 10^{-21}$ cm^2 on the laser line at 1321 nm in π-polarization and $\sigma_{ESA} = 2 \times 10^{-21}$ cm^2 on the emission line at 1313 nm in σ-polarization.

Since Nd:YLF is commonly used as a gain material in Q-switched lasers, ESA losses on the pump wavelength can become important. Figure 7 shows the combined GSA and gain-ESA cross sections between 770 nm and 840 nm in π-polarization. This is the preferred absorption band for diode pumping. The GSA lines in the gain-ESA spectrum are due to the bleaching of the ground state. The reduction of the GSA by bleaching during a pumping cycle appears as a net "gain" in the gain-ESA spectrum because of the increased transmitted intensity; see (1). The GSA lines belong to the transition $^4I_{9/2} \rightarrow {}^4F_{5/2}$. The $^4F_{5/2}$ manifold relaxes nearly completely nonradiatively into the $^4F_{3/2}$ metastable state. Because the relaxation is fast and nonradiative, no stimulated emission can be detected in the region around 800 nm. The signal in the gain-ESA spectrum is exclusively due to the superimposed effects of GSA bleaching and ESA. An independently measured GSA spectrum is presented as a bold line for comparison with the GSA-ESA spectrum in Fig. 7. The differences between the two spectra are caused by ESA. ESA is observed at 803 nm with a cross section of about $\sigma_{ESA} = 6 \times 10^{-21}$ cm^2. On the GSA line at 797 nm the ESA cross section is $\sigma_{ESA} = 3 \times 10^{-21}$ cm^2. On the contrary, no ESA is found on the GSA line at 792 nm that is most suit-

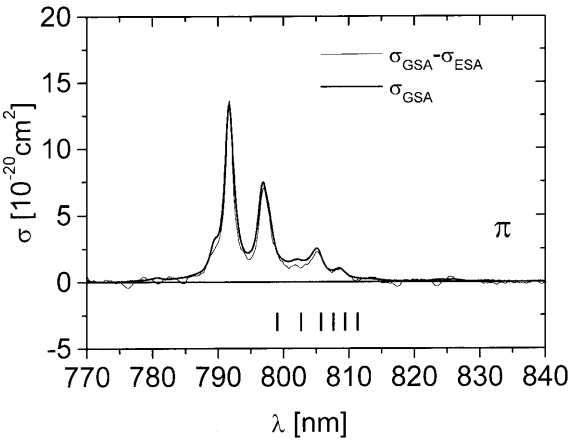

Fig. 7. π-polarized spectrum $\sigma_{GSA} - \sigma_{ESA}$ (*narrow line*) and absorption cross section spectrum σ_{GSA} (*bold line*) of Nd:YLF in the region of the pump band. The resolution of both spectra is 0.8 nm

able for diode pumping. Note that the ESA cross sections in the pumping region given here have a high error margin because of the moderate signal-to-noise ratio of the gain-ESA spectrum. It can however be stated that the ESA cross sections of the ${}^4F_{3/2} \rightarrow {}^2D_{5/2} + {}^2P_{1/2}$ transitions are small, probably because these transitions are spin forbidden.

In [10–13] it was found that nonradiative upconversion processes can become the dominating mechanisms for the population of excited states if a high inversion is reached. In [13] it is stated that under these conditions the ${}^4G_{7/2}$ manifold becomes populated and ESA from this multiplet into the ${}^2P_{3/2}$ manifold around 1.3 μm and into the ${}^4D_{5/2}$ manifold around 1.05 μm becomes possible. This might cause additional losses in the Q-switched mode. However ESA from the ${}^4G_{7/2}$ multiplet is not visible in our spectra, which were measured under moderate excitation. It should therefore induce only small losses in the cw mode and be a minor problem in comparison to upconversion losses in the Q-switched mode.

2.3 Nd:*LSB*

Upconversion losses and lifetime concentration quenching are less a problem in Nd:LSB than in other crystals. LSB can be doped with up to 10 at. % Nd without strong concentration quenching of the ${}^4F_{3/2}$ lifetime due to the large distance between neighbouring lanthanum sites [26]. The Nd ions substitute for the La ions and the electric dipole interaction, which depends sensitively on the distance between neighbouring Nd ions, is strongly reduced in comparison to other crystal hosts.

Nd:LSB shows mainly homogeneously broadened lines with a width of 40 cm^{-1} at 300 K. Inhomogeneous broadening contributes with 10 cm^{-1} and is due to lattice disorder [26].

Figure 8 shows the *x*- and *y*-polarized gain-ESA spectra of monoclinic Nd:LSB. The *x* axis is the indicatrix axis with the highest refractive index ($n_x = 1.8280$ @1000 nm) and is identical to the crystallographic axis with twofold rotation symmetry. The *y* axis is the indicatrix axis with the second highest and *z* the axis with the lowest refractive index ($n_y = 1.8272, n_z = 1.7486$). In *x*- and *y*-polarizations Nd:LSB shows much higher absorption and emission cross sections than in *z*-polarization. Since the *z*-polarized gain-ESA spectrum measured in our setup has a low signal-to-noise ratio and is unimportant from the practical point of view, it is not shown here. The energy values of the various Stark levels of the Nd^{3+} ions in LSB are known only up to 14 000 cm^{-1} [14], so that the exact positions of ESA lines between 850 nm and 1500 nm are uncertain. We estimated the regions of possible ESA from the positions of the GSA bands in the absorption spectra at 300 K and the energy of the ${}^4F_{3/2}$ manifold. The spectral regions, where ESA from the ${}^4F_{3/2}$ manifold is expected are indicated as arrows in Fig. 8.

As shown in Fig. 9 an influence of ESA on the main emission line at 1063 nm can not be derived from the spectra. This is presumably due to the large stimulated emission linewidth of Nd^{3+} ions in LSB. Strong broad stimulated emission lines make the identification of much weaker ESA structures in the same spectral region very difficult. However the typical maximum ESA cross sections around 970 nm and 1040 nm are about 5×10^{-21} cm^2. This value can even be taken as an upper limit for the ESA cross section at 1063 nm.

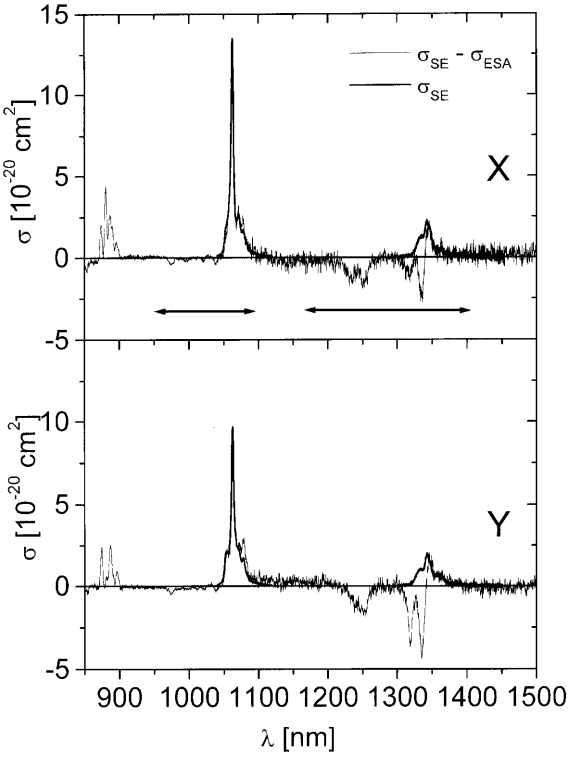

Fig. 8. Polarized gain-ESA spectra $\sigma_{SE} - \sigma_{ESA}$ (*narrow line*) and emission cross section spectra σ_{SE} (*bold line*) of Nd:LSB between 850 nm and 1500 nm. The regions of possible ESA transitions starting from the ${}^4F_{3/2}$ multiplet are indicated by *arrows*

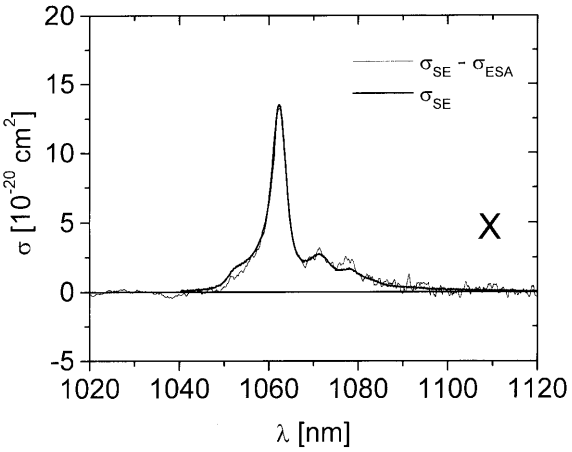

Fig. 9. *x*-polarized gain-ESA spectrum $\sigma_{SE} - \sigma_{ESA}$ (*narrow line*) and emission cross section spectrum σ_{SE} (*bold line*) of Nd:LSB around 1060 nm. The resolution of the gain-ESA spectrum is 0.8 nm, the resolution of the emission cross section spectrum is 0.2 nm

In the *x*-polarized spectrum around 1330 nm, shown in Fig. 10, strong ESA lines are observed with peaks at 1319 nm and 1336 nm. The ESA line at 1336 nm has a peak cross section of about 4×10^{-20} cm^2. This ESA line overlaps with a broad region of stimulated emission (bold line) that exists between 1320 nm and 1370 nm. Effective gain is reached only for wavelengths longer than 1340 nm. Meyn [26] reports that a free-running cw laser was achieved at 1348 nm in *x*-polarization. The slope efficiency of this laser was only 25%. This is a factor of 2 below the theoretical quantum limit

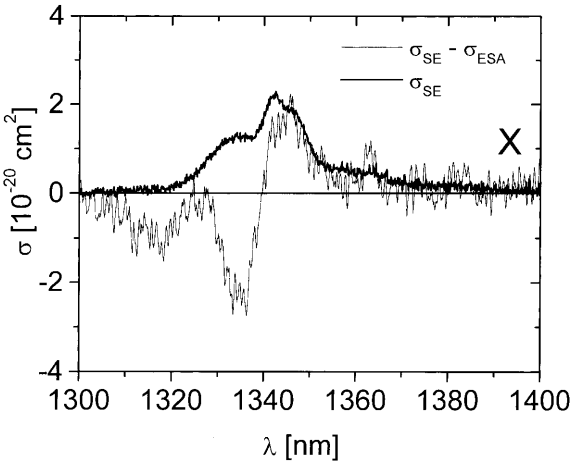

Fig. 10. *x*-polarized gain-ESA spectrum $\sigma_{SE} - \sigma_{ESA}$ (*narrow line*) and emission cross section spectrum σ_{SE} (*bold line*) of Nd:LSB around 1340 nm. The resolution of the gain-ESA spectrum is 1.8 nm, the resolution of the emission cross section spectrum is 0.2 nm

whereas laser operation at 1063 nm was realized with slope efficiencies near to the theoretical limit. This indicates that a wing of the 1336 nm ESA line reduces the laser efficiency at 1348 nm. However, looking at the small differences between the spectra of the combined gain-ESA and of the stimulated emission cross sections at 1348 nm, it seems implausible that ESA is the only reason for this efficiency reduction. Probably amplified spontaneous emission at 1063 nm must be considered as an additional loss mechanism for the 1348 nm laser, too.

3 Summary and outlook

In conclusion Nd^{3+} doped CWO, YLF, and LSB crystals show absorption from the metastable $^4F_{3/2}$ manifold to higher energy states. Peak ESA cross sections are 8×10^{-20} cm^2 (π) at 1054 nm in Nd:CWO, 4×10^{-20} cm^2 (π) at 1052 nm and 10^{-20} cm^2 (σ) at 1048 nm in Nd:YLF, and 5×10^{-20} cm^2 (x) at 1047 nm in Nd:LSB. The ESA cross sections on the main laser lines around 1060 nm are small in all three crystals. At 1330 nm an overlap between the regions of laser emission and ESA is observed in Nd:CWO and Nd:LSB. Both crystals are not suitable for effective laser operation in this wavelength region. In Nd:YLF the emission line in π-polarization at 1321 nm does only negligibly interfere with ESA ($\sigma_{SE} > 20\sigma_{ESA}$@1321 nm).

Neither in Nd:LSB nor in Nd:CWO significant ESA is found on the main emission line near 1060 nm. Other features such as the ratio of inhomogeneous line broadening to homogeneous broadening are more decisive for the laser properties [27].

In Nd:YLF the ESA on the absorption band for diode pumping at 792 nm is negligible. However, losses from upconversion processes should be taken into account in Q-switched operation. ESA might then become possible from higher states than the $^4F_{3/2}$ manifold.

The similarity of the crystal structures of Nd:YLF and Nd:CWO is observed in the gain-ESA spectra. Separated and narrower lines in Nd:YLF allow an analysis whereas ESA is hidden under broadened stimulated emission lines in the gain-ESA spectra of Nd:CWO. To gain further information about the exact ESA spectrum in the regions of strong stimulated emission or GSA in Nd:CWO and Nd:LSB, additional ESE measurements have to be performed and calibrated by the ESA cross section values given in this paper.

References

1. L.F. Johnson, K. Nassau: Proc. Inst. Radio Engineers **49**, 1704 (1961)
2. L.F. Johnson, G.D. Boyd, K. Nassau, R.R. Soden: Phys. Rev. **126**(4), 1406 (1961)
3. L.F. Johnson, R.A. Thomas: Phys. Rev. **131**(5), 2038 (1963)
4. A.A. Kaminskii, L.S. Kornienko, G.V. Maksimova, V.V. Osiko, A.M. Prokhorov, G.P. Shipulo: Sov. Phys. JETP **22**(1), 22 (1966)
5. D.C. Cronemeyer, M.W. Beaubien: Appl. Phys. Lett. **4**(4), 85 (1964)
6. J.R. Ryan, R. Beach: J. Opt. Soc. Am. B **9**(10), 1883 (1992)
7. A.L. Harmer, A. Linz, D. Gabbe, L. Gillespie, G.M. Janney, E. Sharp: Bull. Am. Phys. Soc. **12**, 1068 (1967)
8. E.J. Sharp, D.J. Horowitz, J.E. Miller: J. Appl. Phys. **44**(12), 5399 (1973)
9. A.L. Harmer, A. Linz, D.R. Gabbe: J. Phys. Chem. Solids **30**, 1483 (1969)
10. W. Seelert, H.P. Kortz: OSA Proc. ASSL, Vol. 13, ed. by L.L. Chase, A.A. Pinto, pp. 209–211 (1992)
11. Y. Guyot, H. Manaa, J.Y. Rivoire, R. Moncorgé, N. Garnier, E. Descroix, M. Bon, P. Laporte: Phys. Rev. B **51**(2), 784 (1995)
12. Y. Guyot, R. Moncorgé: J. Appl. Phys. **73**(12), 8526 (1993)
13. T. Chuang, H.R. Verdún: IEEE J. Quantum Electron. **QE-32**(1), 79 (1996)
14. J.P. Meyn, T. Jensen, G. Huber: IEEE J. Quantum Electron. **QE-30**(4), 913 (1994)
15. P.E.-A. Möbert, P. LiKamWa, B.H.T. Chai, G. Huber: OSA proc. ASSL, ed. by C.R. Pollock, W.R. Bosenberg **10**, 455 (1997)
16. N. Faure, C. Borel, M. Couchaud, G. Basset, R. Templier, C. Wyon: Appl. Phys. B **63**, 593 (1996)
17. P.R. Morkel, M.C. Ferries, S.B. Poole: Opt. Commun. **67**(5), 349 (1988)
18. S. Kück, L. Fornasiero, E. Mix, G. Huber: Appl. Phys. B **67**, 151 (1998)
19. L. Fornasiero, S. Kück, T. Jensen, G. Huber: Appl. Phys. B **67**, 549 (1998)
20. S. Zemon, G. Lambert, W. J Miniscalco, R.W. Davies, B.T. Hall, R.C. Folweiler, T. Wei, L.J. Andrews, M.P. Singh: In: Fiber Laser Sources and Amplifiers II, ed. by M.J. Digonnet, Proc. SPIE **1373**, 21 (1991)
21. J. Koetke, G. Huber: Appl. Phys. B **61**, 151 (1995)
22. D.E. McCumber: Phys. Rev. **136**(4A), 954 (1964)
23. A.M. Morozov, M.N. Tolstoi, P.P. Feofilov: Opt. Spectrosc. **22**, 139 (1967)
24. A.S. da Gama, G.F. de Sa, P. Porcher, P. Caro: J. Chem. Phys. **75**(6), 2583 (1981)
25. N. Karayianis: J. Phys. Chem. Solids **32**, 2385 (1971)
26. J.P. Meyn: Ph.D. thesis, Hamburg (1994)
27. N. Mermilliod, R. Romero, I. Chartier, C. Garapon, R. Moncorgé: IEEE J. Quantum Electron. **QE-28**(4), 1179 (1992)